crystals

MDPI

Article

Effects of the Sintering Process on Al_2O_3 Composite Ceramics Fabricated Using Material Extrusion and Photo-Polymerization Combined Process

Xin He [1], Jie Xu [2,*], Lijie He [3] and Weixi Ji [4]

[1] School of Mechatronic Engineering, Jiaxing Nanhu University, Jiaxing 314001, China; 7180832001@stu.jiangnan.edu.cn
[2] Department of Aerospace Science and Technology, Space Engineering University, Beijing 101400, China
[3] Henan Zhongfen Instrument Co., Ltd., Shangqiu 476000, China; 17710099329@163.com
[4] School of Mechanical Engineering, Jiangnan University, Wuxi 214122, China; weixiji_jiangnan@outlook.com
* Correspondence: xujiemechanic@163.com

Abstract: The sintering process can improve the microstructure of Al_2O_3 composite ceramics and enhance their comprehensive properties, but the effects of the sintering process on Al_2O_3 composite ceramics are still unclear. Herein, a novel Al_2O_3 composite ceramic was printed using the material extrusion and photo-polymerization combined process, and the final ceramic was obtained using one-step sintering (TS) and two-step sintering technology (TSS). Based on the testing results, such as the relative density (D_{rel}), average grain size (AGS), hardness, bending strength, and fracture toughness, TSS was suitable for the refinement of commercial Al_2O_3 ceramics. Moreover, the highest sintering temperature of the second step (T_2) was at 1550 °C, while that of the shortest holding time (t) was at 4 h (TSS_8), which was to ensure densification before rapid grain growth. The D_{rel} and AGS of the best ceramics obtained via TSS_8 were 97.65% and 1.52 µm, respectively. Their hardness, bending strength, and fracture toughness were also enhanced, and they were affected by T_2, t, and the interaction. In sum, the TSS obtained better fracture toughness and bending strength, which had great potential in the application of the additive manufacturing field.

Keywords: Al_2O_3 ceramic; sintering technology; material extrusion; photo-polymerization; additive manufacturing

Citation: He, X.; Xu, J.; He, L.; Ji, W. Effects of the Sintering Process on Al_2O_3 Composite Ceramics Fabricated Using Material Extrusion and Photo-Polymerization Combined Process. *Crystals* **2023**, *13*, 1679. https://doi.org/10.3390/cryst13121679

Academic Editor: Vladislav V. Kharton

Received: 4 September 2023
Revised: 4 December 2023
Accepted: 8 December 2023
Published: 13 December 2023

1. Introduction

Al_2O_3 ceramics is one of the most common engineering materials, and its performance depends on the density and control of fine particles [1]. In the technology of obtaining dense and fine particle ceramics, fine particles in raw material will reduce the fluidity of the slurry, which has limited the form of the green body [2,3], and it will hinder the further application of the commercial Al_2O_3. Dense and fine-grained ceramics can be obtained via pulse plasma sintering, liquid-phase sintering, laser sintering, adding additives, etc., but the sintering process is complex, and the cost is high [4–8]. One-step sintering (TS) is common, economical, and easy to operate, which can not only improve compactness through higher sintering temperatures but also promote grain growth [9–11]. The slightly lower sintering temperature can uniformly refine the particles and reduce their compactness [12], which limits the application of ceramic structure densification and refinement.

As ceramic fabrication technology develops, two-step sintering (TSS) is adopted to control the sintering rate and achieve the density and refinement of ceramics [13–15] to improve their mechanical properties [16,17]. Generally, the first step of sintering to the maximum temperature is recorded as T_1. After a brief stay, it quickly cools to T_2 as the second step to sintering temperature and cools down to room temperature after holding temperature for t_2 [18]. The dense Al_2O_3 ceramics [19–21], $BaTiO_3$ ceramics [22], and other ceramics [23,24] are obtained using TSS to inhibit the growth of ceramic grains.

Z. Razavi et al. [25] prepared and characterized sub-micrometer Al_2O_3 ceramics (grain size, 150 nm) using different TSS and discussed the effects of T_1 and t_2 on the densification and grain of ceramics. Compared with TS, when t_2 = 60 h, T_1 goes from 1300 °C to 1150 °C, the grain size in the bulk was reduced from 1.2 μm to 0.85 μm. The grain size decreased to 0.5 μm when T_1 dropped to 1250 °C, and the relative density (D_{rel}) was less than 88% at T_2 = 1100 °C, indicating that temperature played a vital role for TSS, but the period of t_2 was longer, and the effects on average grain size (AGS) and D_{rel} has not been analyzed. N.J. Lóh et al. [26] used this technique to obtain the three commercial Al_2O_3 of different purity (92, 96, and 99 wt% of Al_2O_3), evaluate the effects of T_2 and t_2 on density, and conclude the maximum T_2 (1550 °C) and minimum t_2 (4 h). Moreover, the interaction of T_2 and t_2 significantly impacted the density of 99.7 wt% Al_2O_3 (particle size = 0.73 μm) [27]. However, the systematic evaluation of sintering parameters on compactness, AGS, and mechanical properties are still unclear, and the AGS is within the range of sub-micrometer (150–200 nm) and micrometer (0.73–2.16 μm), the application of TSS in multi-components of micro-nanometer particles composite ceramics has not been analyzed.

In this study, Al_2O_3, TiCN, and the other micro-nanometer particles were used as raw powder. The ceramic green body was fabricated via material extrusion and the photo-polymerization combined process (MEX-PPM) [28], and using two-step degreasing [29] and TSS, the final ceramic parts. The effect of the sintering process on Al_2O_3 composite ceramics fabricated using the MEX-PPM process was studied through Drel, AGS, mechanical properties, and microstructure measurements.

2. Materials and Methods

2.1. Materials

Al_2O_3 (Tuopu Metal Materials Co., Ltd., Suzhou, China) was used as the matrix material, TiCN as the additive, MgO as the sintering additive, Ni and Mo as the metal binder (Tuopu Metal Materials Co., Ltd., Suzhou, China), 0.15 wt% oleic acid (OA) as the surfactant [28], and 1,6-hexanediol diacrylate (HDDA) (Changxing Chemical Co., Ltd., Shanghai, China) as the prepolymer solution. Diphenyl (2,4,6-trimethylbenzoyl)-phosphate oxide (TPO) (BASF GmbH, Shanghai, China) was used as a photoinitiator. The properties and content of raw materials are listed in Table 1.

Table 1. Properties and content of raw materials [30].

Components	Grain Size (μm)	Theoretical Density (g/cm^3)	Content (wt%)
Al_2O_3	1 μm	3.98	54
Al_2O_3	200 nm	3.98	10
TiCN	1 μm	5.08	30
Ni	1 μm	9.90	2
Mo	1 μm	10.20	2
MgO	1 μm	3.58	2

2.2. Preparation Process

The preparation of ceramic slurry for the MEX-PPM process can be divided into three steps: modifying ceramic powder, preparing prepolymer solution, and mixing slurry. Firstly, the ceramic powder was added to deionized water containing OA, mixed evenly, and dried to obtain the modified powder. Then, the modified ceramic powder was added into the HDDA prepolymer solution with TPO and milled for 4 h. Finally, the milled slurry was subjected to ultrasonic vibration to eliminate bubbles in the slurry, and the available ceramic slurry was obtained.

In the process of printing ceramic bulk using the MEX-PPM process, the ceramic slurry is extruded through the round nozzle and deposited on the workbench, which receives UV light radiation to maintain the shape and prevents the collapse and deformation of the deposited slurry caused by gravity [31]. The round nozzle and UV light source are fixed on the equipment. The 3D printing software slices the parts to generate a G-code, drives

the workbench to move, and obtains the final ceramic bulk through the layer-by-layer deposition of slurry and UV light curing. The schematic diagram of the MEX-PPM process is shown in Figure 1.

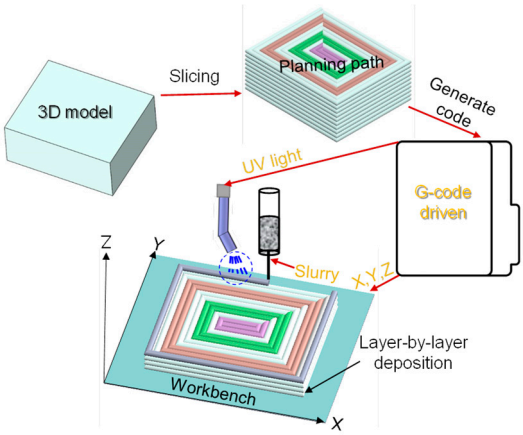

Figure 1. Schematic diagram of the MEX-PPM process.

The above MEX-PPM process was used to print the dense ceramic bulk at a printing speed of 5 mm/s and a radiation energy of 20 J/cm^3 at room temperature and obtain the final ceramic parts through degreasing and sintering technology.

2.3. Degreasing and Sintering Process

2.3.1. Degreasing Process

This work adopted a two-step degreasing (TSD) with a controllable pyrolysis rate [29] to remove the organic binder HDDA in the ceramic bulk; the TSD process is shown in Figure 2.

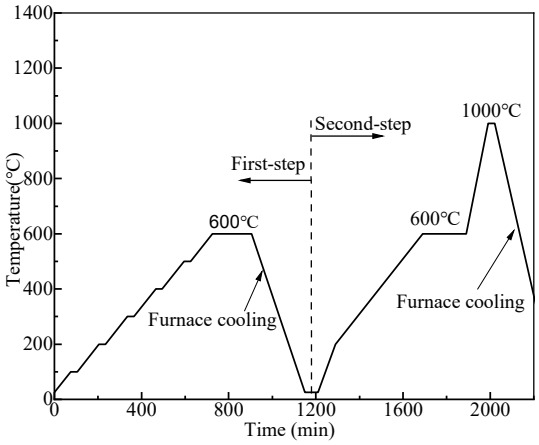

Figure 2. TSD process.

Combined with the experimental conditions, the first step of degreasing in this study was carried out in a tubular furnace (GSL-1700X, Hefei Kejing Material Technology Co., Ltd., Hefei, China) at the rate of 1 °C/min. The temperature was hold for 30 min every 100 °C increased, hold for 180 minutes when it reaches 600 °C, and then the furnace was then cooled to room temperature. The second step of degreasing was carried out in an air furnace, which was heated to 200 °C, 600 °C (holding for 200 min), and 1000 °C (holding for 30 min) at 2 °C/min, 1 °C/min, and 4 °C/min, respectively, and then the furnace was cooled to room temperature to complete the whole degreasing process.

2.3.2. Sintering Process

After degreased Al_2O_3 composite ceramic adopts the traditional TS and the designed TSS to obtain the final ceramic parts, the process of TS and TSS is shown in Figure 3.

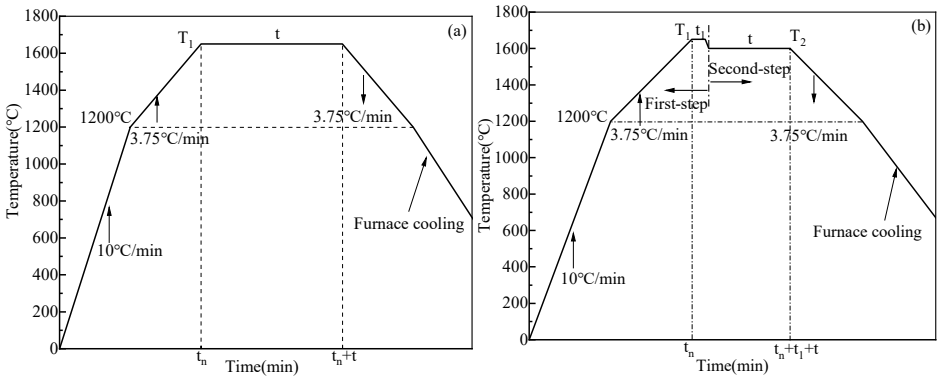

Figure 3. (**a**) TS sintering process and (**b**) TSS sintering process.

Figure 3a shows the changing curve of sample TS. Firstly, the temperature was raised to 1200 °C at a rate of 10 °C/min, then it was increased to T_1 at a rate of 3.75 °C/min. After that, the temperature was cooled to 1200 °C with a rate of 3.75 °C/min. Finally, the temperature was cooled down to room temperature. As shown in Figure 3b, the changing curve of TSS is similar to that of TS in the initial stage and then stays briefly after heating to the maximum temperature of T_1, and then it is cooled down to T_2 at a rate of 50 °C/min, and holding at t for a certain time. While the other temperature-controlling procedures were the same as that of TS, TSS sintering technology was carried out with two factors and three levels. The specific sintering parameters are shown in Table 2.

Table 2. The specific parameters of TSS and TS sintering.

Sintering Process	T_1/°C	T_2/°C	t/h
TSS_1	1500	1450	2
TSS_2	1500	1450	4
TSS_3	1500	1450	6
TSS_4	1550	1500	2
TSS_5	1550	1500	4
TSS_6	1550	1500	6
TSS_7	1600	1550	2
TSS_8	1600	1550	4
TSS_9	1600	1550	6
TS	1650	/	4

Notes: The sintering process is carried out in a high-temperature tube furnace with argon gas.

2.4. Characterizations of the Prepared Samples

To evaluate the properties of Al_2O_3 composite ceramic obtained by various sintering technologies, the ceramic sample was obtained by cutting, polishing with diamond particles, cleaning, drying, and gold spraying. The density was measured using the Archimedes drainage method; the microstructure was characterized using a scanning electron microscope (SEM, Evo18, Zeiss, Oberkochen, BW, Germany), and the grain size was measured using the line intercept method. The hardness, fracture, and toughness were measured using a Vickers hardness tester (HV-1000ZCM-XY, Anyi Instrument Co., Ltd., Shanghai, China), and the three-point bending test was carried out using an electronic universal testing machine (WDW-100KN, Instron Co., Boston, MA, USA). The fracture toughness and bending strength of ceramic specimens were obtained from Formulas (1) and (2), respectively.

$$KIC = 0.203 \times 1.8544\ P/(4C^{3/2}) \quad (1)$$

where P is the pressure load, and C is the average crack length.

$$\sigma = (3F \times L)/(2b \times h^2) \quad (2)$$

where F is the failure load, L is the span, and b and h are the width and thickness of the specimen, respectively.

In addition, the density, particle size, and mechanical properties of the ceramics were characterized using an average of seven tests per sample out of 20 samples from the same batch.

3. Results and Discussion

3.1. Comparison of Results from TSS and TS

The TS and TSS were applied to Al_2O_3 composite ceramics, and the D_{rel} and AGS of ceramic sintered bodies were obtained, as shown in Figure 4.

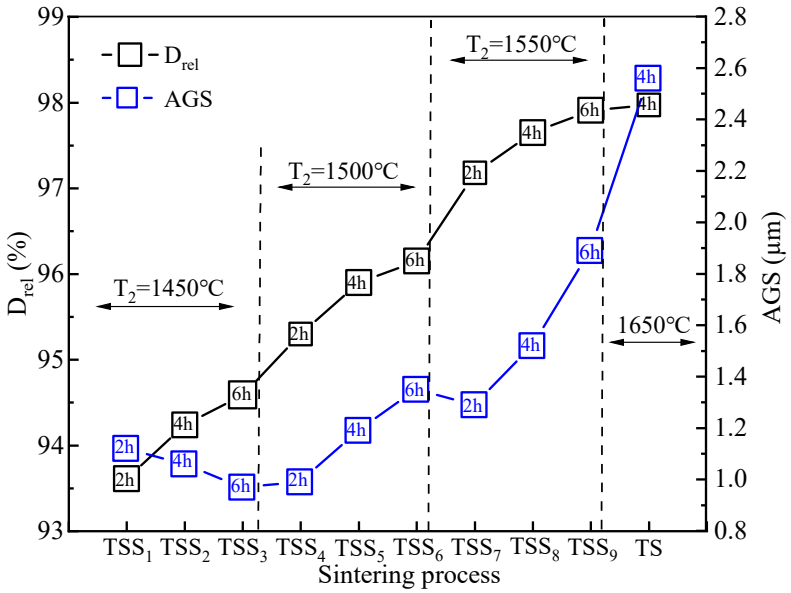

Figure 4. The D_{rel} and AGS of Al_2O_3 composite ceramics treated with TSS and TS.

Figure 4 shows the D_{rel} (black mark) and AGS (blue mark) of Al_2O_3 composite ceramics under the action of each TSS and TS. The same holding time t = 4 h, the D_{rel} (TSS_8) (97.65%) obtained via TSS is slightly lower than that of TS (97.97%), but the AGS (TSS_8) (1.52 μm) is significantly lower than TS (2.56 μm). With the increase in t to 6 h, the D_{rel} (TSS_9) (97.91%) treated via TSS is close to TS, and the increased AGS (1.89 μm) is still lower than that of TS. Although the D_{rel} of other ceramics (93.61–97.18%) treated with TSS is lower than that of TS, their AGS (1.12–1.29 μm) is significantly lower than that of TS. TSS is more beneficial to Al_2O_3 composite ceramics from the compactness and grain refinement point of view.

In addition, the D_{rel} and AGS increase the amount of ceramic obtained via TSS with the T_2. When t = 2 h, T_2 from 1450 °C increases to 1550 °C, causing the D_{rel} from 93.61% to increase to 97.18% and the AGS from 1.12 μm to increase to 1.52 μm. When the t increases, the change in compactness is not always obvious, and the AGS still grows. At T_2 = 1550 °C, t from 2 h increased to 4 h, the D_{rel} from 97.18% (TSS_7) to 97.65% (TSS_8), and the AGS rapidly from 1.29 μm to 1.52 μm. The t increased to 6 h, the D_{rel} increased to 97.91%, and the AGS increased to 1.89 μm. Slightly lower T_2 ensures fine-grained ceramics; the changing compactness leads to different mechanical properties, as shown in Figure 5.

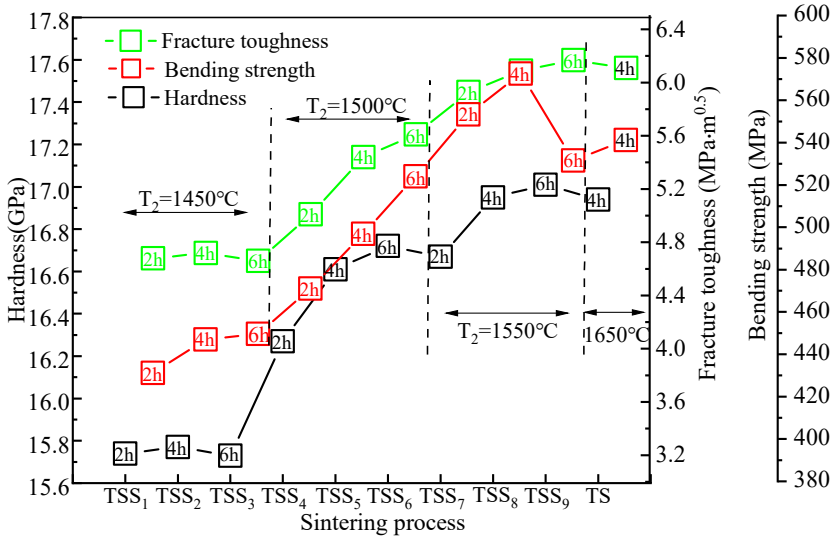

Figure 5. The mechanical properties of Al_2O_3 composite ceramics treated via TSS and TS.

Figure 5 shows the mechanical properties of Al_2O_3 composite ceramics; the black, red, and green marks correspond to hardness, bending strength, and fracture toughness, respectively. Good ceramic hardness and fracture toughness can be obtained under the sintering conditions of T_2 = 1550 °C and t = 6 h (TSS_9), which are 17.01 GPa and 6.17 MPa·$m^{0.5}$, respectively. The t was shortened to 4 h, and the ceramics obtained via TS (16.94 GPa, 6.11 MPa·$m^{0.5}$) at 1650 °C were equivalent to TSS_8 (16.95 GPa, 6.09 MPa·$m^{0.5}$) at 1550 °C. The bending strength obtained via TSS_7 (553.34 MPa) at 1550 °C for 2 h is higher than TS (541.23 MPa).

The mechanical properties of ceramic are improved with the T_2. When T_2 from 1450 °C to 1550 °C at t = 2 h, the hardness, bending strength, and fracture toughness increased from 15.74 GPa, 431.14 MPa, and 4.68 MPa·$m^{0.5}$ to 16.67 GPa, 553.34 MPa, and 5.93 MPa·$m^{0.5}$, respectively. But, the mechanical properties do not improve significantly with the increase in t. For example, the hardness at T_2 = 1550 °C, t = 4 h (TSS_8), and t = 6 h (TSS_9) are close, the fracture toughness increases slowly, and the bending strength decreases.

The fine particles of dense ceramics can be obtained under the T_2 = 1550 °C, t = 4 h or 6 h (Figure 4), and the mechanical properties under the T_2 = 1550 °C, t = 4 h (Figure 5) are close to TS. So, the sintering parameter for obtaining the best Al_2O_3 composite ceramics is TSS_8 with T_2 = 1550 °C, t = 4 h. Using the TSS_8 process, the D_{rel}, AGS, hardness, bending strength, and fracture toughness were 97.65%, 1.52 μm, 16.95 GPa, 572.59 Mpa, and 6.09 MPa·$m^{0.5}$. The above results preliminarily show that the T_2 and t in TSS have varying degrees of effect on the properties of Al_2O_3 composite ceramics. The impact and reliability of the T_2 and t on the properties of ceramics need to be further analyzed through data statistics.

3.2. Effects of T_2 and t on Al_2O_3 Composite Ceramics

The reliability of the impact of factors (T_2 and t) on variables (D_{rel}, AGS, and mechanical properties) was evaluated using SPSS software. In the statistical analysis, the adjusted R^2 is used to assess the fitting degree of the model, and the standard effect quantity (η^2) and *p*-value are used to evaluate the degree and significance of the effects of T_2 and t on ceramic properties, respectively. It is assumed that when *p*-value < 0.05, the factors have significant effects on variables. On the contrary, the effect of factors on variables is not significant.

3.2.1. Effects of T_2 and t on D_{rel} and AGS

The statistical analysis results of T_2 and t for D_{rel} and AGS are shown in Table 3, which shows the effects of T_2, t, and their interaction (T_2 by t) on the D_{rel} of Al_2O_3 composite

ceramics. The adjusted R^2 is 0.994, which indicates that the linear regression model has a high degree of fit. The *p*-value of T_2 (0.0016288) and t (0.0029354) is less than 0.05, and the *p*-value of interaction between both T_2 and t (0.6149418) is more than 0.05, which indicates that D_{rel} is only affected by individual T_2 and t. Moreover, T_2 (η^2 = 0.9861565) has a stronger impact on drel than t (η^2 = 0.9639632). Figure 6a shows the interaction between T_2 and t for D_{rel}. Figure 6a indicates that there is no interaction between T_2 and t because the three kinds of sintering temperatures at holding for 2, 4, and 6 h are approximately parallel in the t vs. D_{rel} curve.

Table 3. The effects of T_2 and t on D_{rel}.

Variable	Factor	η^2	*p*-Value	The Adjusted R^2
D_{rel}	T_2	0.9861565	0.0016288	0.994
	t	0.9639632	0.0029354	
	T_2 by t_2	0.2768595	0.6149418	

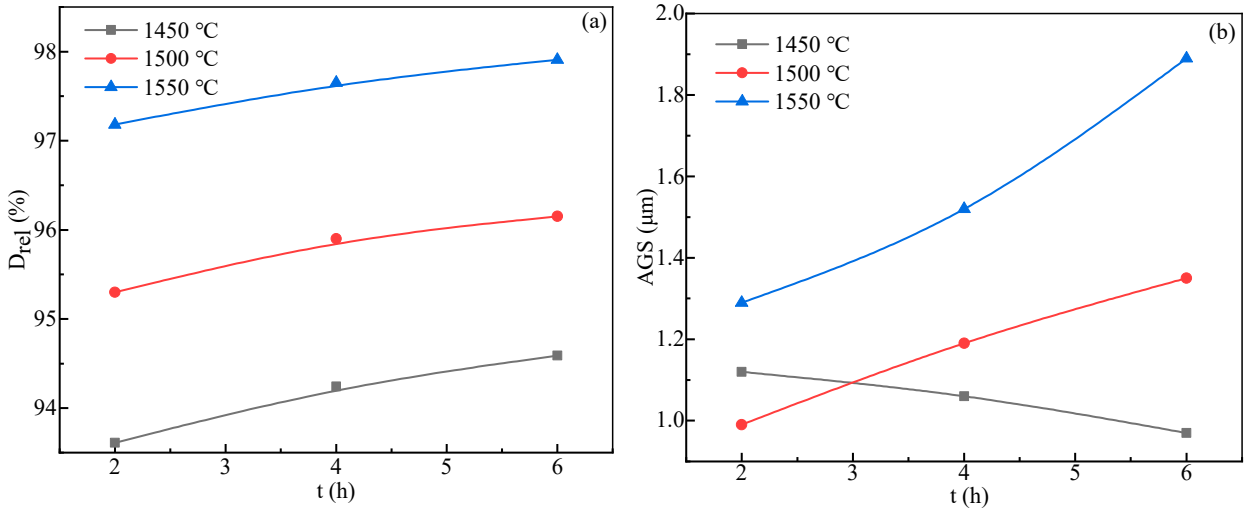

Figure 6. The interaction of T_2 by t. (**a**) Effect of T2 by t on Drel. (**b**) Effect of T2 by t on AGS.

Table 4 shows the effects of T_2, t, and their interaction on the AGS of Al_2O_3 composite ceramics. The adjusted R^2 = 0.986 indicates that the static models are valid. The η^2 of T_2, t, and their interaction gradually rose 0.8967313, 0.9674137, and 0.9755070, and their *p*-values were less than 0.5. The results show that the above factors had a significant impact on the AGS. However, the interaction of both T_2 and t is stronger, followed by T_2 and t. Figure 6b shows the interaction between the T_2 and t for AGS. Figure 6b indicates that there is an interaction between the T_2 and t because an intersection of the lines is observed.

Table 4. The effects of T_2 and t on AGS.

Variable	Factor	η^2	*p*-Value	The Adjusted R^2
AGS	T_2	0.8967313	0.0331859	0.986
	t	0.9674137	0.0025214	
	T_2 by t	0.9755070	0.0038332	

3.2.2. Effects of T_2 and t on Mechanical Properties

The T_2 and t can be applied to the densification and refinement of Al_2O_3 composite ceramics to promote the mechanical properties. The statistical analysis of its effect on mechanical properties is shown in Tables 5–8. The adjusted R^2 are 0.978, 0.995, and 0.995 (0.918), respectively, which indicates that the statistic models are suitable.

Table 5. The effects of T_2 and t on hardness.

Variable	Factor	η^2	*p*-Value	The Adjusted R^2
Hardness	T_2	0.8813812	0.0408536	0.978
	t	0.8513854	0.0254951	
	T_2 by t	0.7652519	0.1137373	

Table 6. The effects of T_2 and t on fracture toughness.

Variable	Factor	η^2	*p*-Value	The Corrected R^2
Fracture toughness	T_2	0.9608961	0.0077327	0.995
	t	0.9060330	0.0125882	
	T_2 by t	0.8801710	0.0414804	

Table 7. The effects of T_2 and t on bending strength.

Variable	Factor	η^2	*p*-Value	The Corrected R^2
Bending strength	T_2	0.8996170	0.0318046	0.918
	t	0.2580958	0.2580958	
	T_2 by t	0.1742553	0.1742553	

Table 8. The effects of T_2 and t on bending strength (Excluding T_2 = 1550 °C, t = 6 h).

Variable	Factor	η^2	*p*-Value	The Corrected R^2
Bending strength	T_2	0.9829973	0.0170027	0.995
	t	0.9715431	0.0143312	
	T_2 by t	0.9105670	0.0894330	

Table 5 presents the impact of T_2, t, and their interaction. Both T_2 (*p*-value = 0.0408536) and t (*p*-value = 0.0254951) significantly affect hardness. However, their interaction is not significant (*p*-value > 0.05). Moreover, T_2 has a stronger impact on hardness than t (0.8813812 against 0.8513854). Figure 7a shows the interaction between the T_2 and t for hardness. Figure 7a confirms that there is no impact on interaction between T_2 and t on hardness because the lines are approximately parallel, as shown in Table 5. In addition, the curve slope is approximately zero at T_2 = 1450 °C, which is caused by lower temperature.

Table 6 presents the impact of T_2 and t on fracture toughness. It is observed that T_2, t, and their interaction individually affect the fracture toughness and *p*-values of 0.0077327, 0.0125882, and 0.0414804, respectively. However, the T_2 has a more significant effect (η^2 = 0.9608961), followed by t and their interaction. Figure 7b shows the interaction between T_2 and t for fracture toughness.

Table 7 presents the *p*-value of T_2, which is less than 0.05. It is observed that T_2 individually affects bending strength, which obviously contradicts the previous research results (Figure 5). Table 8 shows the impact of T_2 and t on bending strength (excluding the data of 1550 °C for 6 h). It is observed that T_2 and t individually affect the bending strength and *p*-values of 0.0170027 and 0.0143312, respectively. Moreover, Figure 7c shows that the curves at T_2 = 1550 °C and t $\leq$ 4 h are almost parallel to each other, and then there is a cross trend at T_2 = 1550 °C, t = 6 h. Therefore, T_2 = 1550 °C and t = 6 h are unsuitable for sintering composite ceramics, which is consistent with the results shown in Figures 4 and 5.

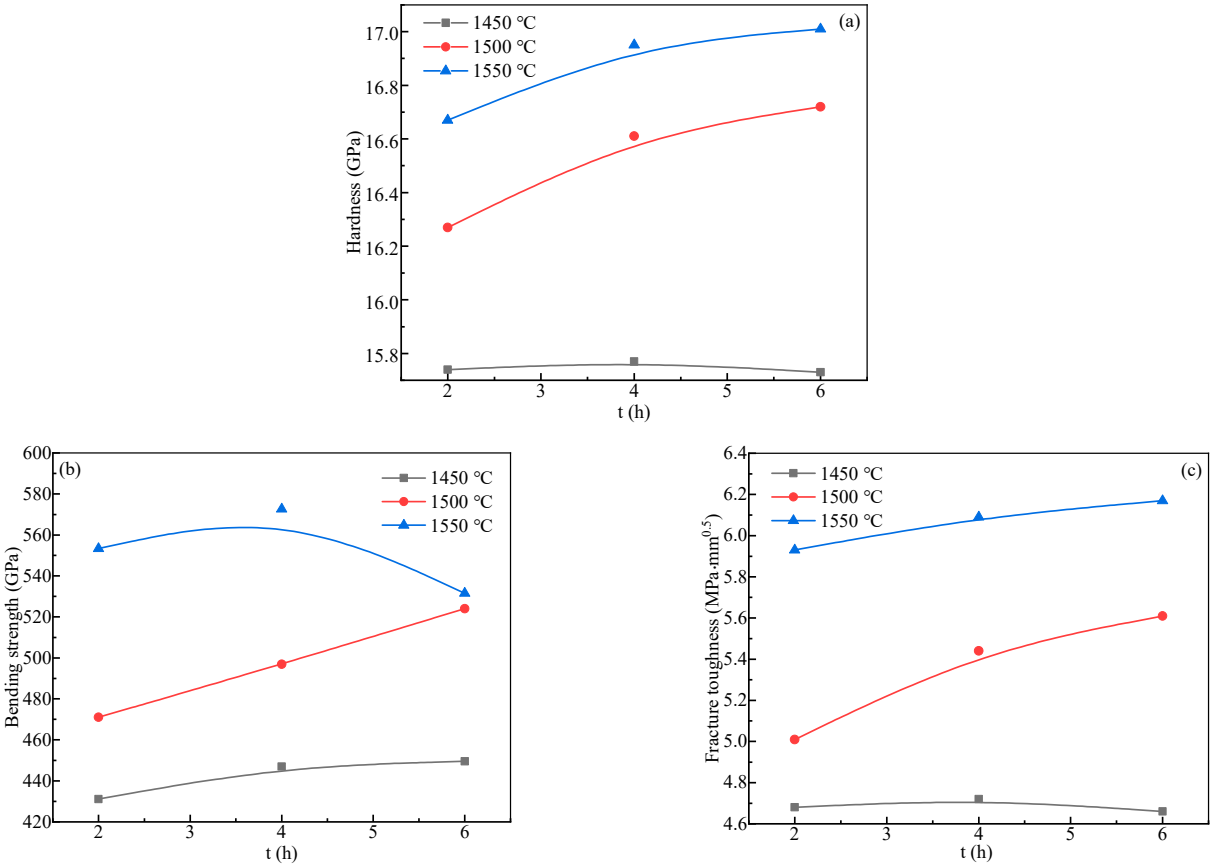

Figure 7. Interaction between T_2 and t (T_2 by t). (**a**) Effect of T_2 by t on hardness. (**b**) Effect of T_2 by t on fracture toughness. (**c**) Effect of T_2 by t on bending strength.

3.2.3. Microstructure of Sintered Ceramics

The performance of Al_2O_3 composite ceramics depends on the microstructure. This work verifies the advantages of TSS from the micro-level by comparing the microstructure of Al_2O_3 composite ceramics acted by TS and the TSS_8, as shown in Figure 8.

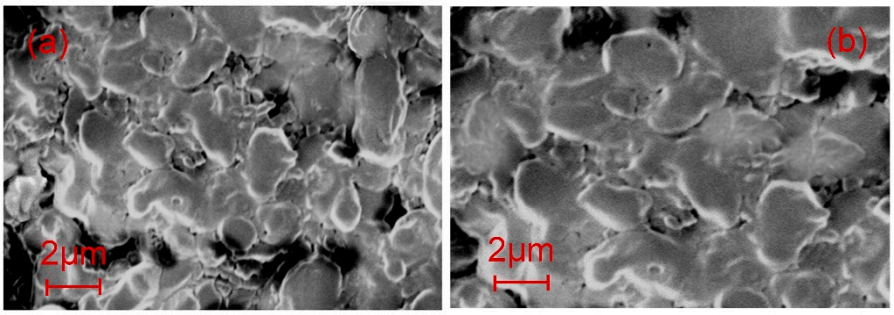

Figure 8. The microstructure of Al_2O_3 composite ceramic acted by (**a**) TSS_8 and (**b**) TS.

Figure 8a,b shows the microstructure of Al_2O_3 composite ceramics obtained via TSS_8 at T_2 = 1550 °C, t = 4 h, and TS at 1650 °C, t = 4 h, respectively. It is found that the ceramic grains obtained via TSS_8 are obviously smaller than those obtained via TS. However, there are small gaps between the grains, which results in lower compactness of ceramics obtained by TSS_8. The microstructure shown in Figure 8 is consistent with the results of D_{rel} and AGS shown in Figure 4. The above results show that the Al_2O_3 composite ceramics obtained via TSS_8 are significantly better than TS; although its compactness is slightly low, the fine-grained ceramics obtained at low cost can bring good comprehensive properties, especially

the bending strength and fracture toughness that determine the engineering properties of ceramics.

4. Conclusions

In this work, an Al_2O_3 composite ceramic was prepared using the MEX-PPM combined process, and the final ceramic samples were obtained via TS and TSS. The effects of sintering processes on Al_2O_3 composite ceramics were studied using experiments, and we conclude the following:

(1) Compared to TS, TSS effectively refined grain size and improved its comprehensive properties. TSS_8 can ensure the densification of ceramic before the rapid grain growth; its highest sintering temperature and shortest holding time were T_2 = 1550 °C and t = 4 h, respectively. Under this condition, the D_{rel} and AGS of the ceramics were 97.65% and 1.52 μm. Their hardness, bending strength, and fracture toughness were 16.95 GPa, 572.59 Mpa, and 6.09 MPa·$m^{0.5}$;

(2) Both T_2 and t and their interactions individually affect the AGS, fracture toughness, and bending strength significantly, although T_2 has more impact. However, both T_2 and t affect the D_{rel} and hardness more significantly.

In addition, the microstructure of ceramics obtained via the TSS_8 and TS was compared, and the advantages of TSS8 from the microscopic point of view were verified. Commercial Al_2O_3 ceramics with good fracture toughness and flexural strength via TSS will have unique advantages in engineering applications.

Author Contributions: Conceptualization, X.H. and J.X.; methodology, X.H. and L.H.; formal analysis, X.H., J.X., W.J. and L.H.; writing—original draft preparation, X.H.; writing—review and editing, X.H., W.J. and J.X.; supervision, J.X., L.H. and X.H. All authors have read and agreed to the published version of the manuscript.

Funding: This research was funded by the National Natural Science Foundation of China (Grant No. 51805212), Natural Science Found of Jiangsu Province (Grant No. BK20160182) and the Major Scientific and the Technological Innovation Project of Shandong Province (Grant No. 2019JZZY020111).

Data Availability Statement: Data are available upon request from the corresponding author.

Conflicts of Interest: The authors declare that they have no competing interest.

References

1. Medvedovski, E. Wear-resistant engineering ceramics. *Wear* **2001**, *249*, 821–828. [CrossRef]
2. Chen, Z.; Li, J.; Liu, C.; Liu, Y.; Zhu, J.; Lao, C. Preparation of high solid loading and low viscosity ceramic slurries for photopolymerization-based 3D printing. *Ceram. Int.* **2019**, *45*, 11549–11557. [CrossRef]
3. Sun, C.; Tian, X.; Wang, L.; Liu, Y.; Wirth, C.M.; Günster, J.; Li, D.; Jin, Z. Effect of particle size gradation on the performance of glass-ceramic 3D printing process. *Ceram. Int.* **2017**, *43*, 578–584. [CrossRef]
4. Guo, H.; Guo, J.; Baker, A.; Randall, C.A. Hydrothermal Assisted Cold Sintering Process: A New Guidance for Low Temperature Ceramic Sintering. *ACS Appl. Mater. Interfaces* **2016**, *8*, 20909–20915. [CrossRef] [PubMed]
5. Guo, H.; Baker, A.; Guo, J.; Randall, C.A. Protocol for Ultralow-Temperature Ceramic Sintering: An Integration of Nanotechnology and the Cold Sintering Process. *ACS Nano* **2016**, *10*, 10606–10614. [CrossRef]
6. Sofia, D.; Chirone, R.; Lettieri, P.; Barletta, D.; Poletto, M. Selective laser sintering of ceramic powders with bimodal particle size distribution. *Chem. Eng. Res. Des.* **2018**, *136*, 536–547. [CrossRef]
7. Song, S.; Gao, Z.; Lu, B.; Bao, C.; Zheng, B.; Wang, L. Performance optimization of complicated structural SiC/Si composite ceramics prepared by selective laser sintering. *Ceram. Int.* **2020**, *46*, 568–5575. [CrossRef]
8. Feng-You, L.; Yu-Ying, L.; Ling, Z.; Xin, S.; Zhi-Hao, Z.; Huan, Z. Effect of TiO_2 Sintering Additives on Alumina Ceramic Prepared with Nano-η-Al_2O_3. *J. Synth. Cryst.* **2019**, *48*, 699–704.
9. Wen, J.; Wang, H.; Fan, L.; Peng, K.; Su, L. Non-additive sintering of Si_2N_2O ceramic with enhanced high-temperature strength, oxidation resistance, and dielectric properties. *Ceram. Int.* **2021**, *47*, 25689–25695. [CrossRef]
10. Yan, D.; Xu, X.; Lu, H.; Wang, Y.; Liu, P.; Zhang, J. Fabrication and properties of Y2O3 transparent ceramic by sintering aid combinations. *Ceram. Int.* **2016**, *42*, 16640–16643. [CrossRef]
11. Wu, Z.; Liu, W.; Wu, H.; Huang, R.; He, R.; Jiang, Q.; Chen, Y.; Ji, X.; Tian, Z.; Wu, S. Research into the mechanical properties, sintering mechanism and microstructure evolution of Al_2O_3-ZrO_2 composites fabricated by a stereolithography-based 3D printing method. *Mater. Chem. Phys.* **2018**, *207*, 1–10. [CrossRef]

12. Palmero, P.; Lombardi, M. Influence of the firing parameters on the phase development and microstructural evolution. *J. Therm. Anal. Calorim.* **2009**, *97*, 191–196. [CrossRef]
13. Lóh, N.J.; Simão, L.; Faller, C.A.; De Noni, A.; Montedo, O.R.K. A review of two-step sintering for ceramics. *Ceram. Int.* **2016**, *42*, 12556–12572. [CrossRef]
14. Wang, X.-H.; Chen, P.-L.; Chen, I.W. Two-Step Sintering of Ceramics with Constant Grain-Size, I. Y_2O_3. *J. Am. Ceram. Soc.* **2006**, *89*, 431–437. [CrossRef]
15. Lukić, M.; Stojanović, Z.; Škapin, S.D.; Maček-Kržmanc, M.; Mitrić, M.; Marković, S.; Uskoković, D. Dense fine-grained biphasic calcium phosphate (BCP) bioceramics designed by two-step sintering. *J. Eur. Ceram. Soc.* **2011**, *31*, 19–27. [CrossRef]
16. Farhandi, H.; Karim, M.N.; Almeida RS, M.; Tushtev, K.; Rezwan, K. Increasing the tensile strength of oxide ceramic matrix mini-composites by two-step sintering. *J. Am. Ceram. Soc.* **2022**, *105*, 1928–1938. [CrossRef]
17. Kim, H.S.; Oh, S.T.; Do Kim, Y. Effects of the two-step sintering process on the optical transmittance and mechanical strength of polycrystalline alumina ceramics. *Ceram. Int.* **2014**, *40*, 14471–14475. [CrossRef]
18. Lin, F.J.T.; Jonghe, L.C.D. Microstructure refinement of sintered alumina by a two-step sintering technique. *J. Am. Ceram. Soc.* **1997**, *80*, 2269–2277. [CrossRef]
19. Bodišová, K.; Šajgalík, P.; Galusek, D.; Švančárek, P. Two-Stage Sintering of Alumina with Submicrometer Grain Size. *J. Am. Ceram. Soc.* **2007**, *90*, 330–332. [CrossRef]
20. Maca, K.; Pouchly, V.; Zalud, P. Two-Step Sintering of oxide ceramics with various crystal structures. *J. Eur. Ceram. Soc.* **2010**, *30*, 583–589. [CrossRef]
21. Li, J.; Ye, Y. Densification and Grain Growth of Al_2O_3 Nanoceramics During Pressureless Sintering. *J. Am. Ceram. Soc.* **2006**, *89*, 139–143. [CrossRef]
22. Moon, S.M.; Wang, X.; Cho, N.H. Nanostructural and physical features of $BaTiO_3$ ceramics prepared by two-step sintering. *Ceram. Soc. Jpn.* **2009**, *117*, 729–731. [CrossRef]
23. Li, X.; Liu, C.; Sun, B.; Liu, X.; Zuo, Z.; Shu, Y.; Zeng, X.; Yi, J.; Chen, H.; Liu, Y.; et al. Refined grain size of ITO ceramic targets prepared by pressure slip casting and two-step sintering. *J. Eur. Ceram. Soc.* **2021**, *4*, 3501–3511. [CrossRef]
24. Hong, D.; Yin, Z.; Yan, S.; Xu, W. Fine grained Al_2O_3/SiC composite ceramic tool material prepared by two-step microwave sintering. *Ceram. Int.* **2019**, *45*, 11826–11832. [CrossRef]
25. Razavi Hesabi, Z.; Haghighatzadeh, M.; Mazaheri, M.; Galusek, D.; Sadrnezhaad, S.K. Suppression of grain growth in sub-micrometer alumina via two-step sintering method. *J. Eur. Ceram. Soc.* **2009**, *29*, 1371–1377. [CrossRef]
26. Lóh, N.J.; Simão, L.; Jiusti, J.; De Noni, A.J.; Montedo OR, K. Effect of temperature and holding time on the densification of alumina obtained by two-step sintering. *Ceram. Int.* **2017**, *43*, 8269–8275. [CrossRef]
27. Lóh, N.J.; Simão, L.; Jiusti, J.; Arcaro, S.; Raupp-Pereira, F.; De Noni, A.; Montedo, O.R.K. Densified alumina obtained by two-step sintering: Impact of the microstructure on mechanical properties. *Ceram. Int.* **2020**, *46*, 12740–12743. [CrossRef]
28. He, X.; Xu, J.; Ji, W. The effect of surfactants on the performances of ceramic slurry by material extrusion and photo-polymerization combined molding process. *J. Ceram. Soc. Jpn.* **2021**, *129*, 489–495. [CrossRef]
29. Zhou, M.P.; Liu, W.; Wu, H.D.; Song, X.; Chen, Y.; Cheng, L.X.; He, F.P.; Chen, S.X.; Wu, S.H. Preparation of a defect-free alumina cutting tool via additive manufacturing based on stereolithography-Optimization of the drying and debinding processes. *Ceram. Int.* **2016**, *42*, 11598–11602. [CrossRef]
30. He, X.; Xu, J.; Ji, W. Effects of n-Al_2O_3 and μ-TiCN on Microstructure and Mechanical Properties of Al_2O_3 Composite Ceramics Manufactured by Material Extrusion and Photo-Polymerization Combined Process. *Crystals* **2022**, *12*, 745. [CrossRef]
31. Liu, Z.; Bhandari, B.; Prakash, S.; Mantihal, S.; Zhang, M. Linking rheology and printability of a multicomponent gel system of carrageenan-xanthan-starch in extrusion based additive manufacturing. *Food Hydrocoll.* **2019**, *87*, 413–424. [CrossRef]